In situ examination of engineered local additives in cement paste via neutron-based scattering techniques

Kunal Kupwade-Patil, Ali Bumajdad, Terrence J. Udovic, Kenneth C. Littrell, Oral Büyüköztürk

ABSTRACT

This work investigates the effect of early-age hydration on microstructural evolution of cement paste with local volcanic ash using neutron-based beamline techniques. Early-age hydration dynamics of Portland cement paste with volcanic ash was examined via Inelastic Neutron Scattering (INS), while the evolution of microstructure was observed with Small Angle Neutron Scattering (SANS). The data obtained from the ratio of Volume Fractal to Surface Fractal clearly showed that greater than 30 % substitution of volcanic ash leads to unreacted volcanic ash and coarser morphology, which could influence the chemo-mechanical properties of the resulting hydration products. INS results showed that the effect of finer-particle-sized volcanic ash contributes to uniform hydration, which accommodates higher conversion of free water to bound water. Such advanced beamline characterization techniques were found useful in providing critical insights into the effect of additives by considering water dyamics along with morphological information during the course of hydration. The multi-scale analysis that combines a time-resolved study of water dynamics along with microstructure is found to provide a basis for optimizing and effectively utilizing engineered additives for the local cement industry.

1. INTRODUCTION

Next-generation synchrotron and neutron-based experimental techniques are becoming increasingly popular to characterize cement-based materials (Biernacki et al., 2017). Spallation sources and high-flux isotope reactors are used to produce the high-intensity neutron beam that can decipher the multi-scale morphology when the cement paste hydrates. Neutron-based experiments for understanding hydration behaviour of ordinary Portland cements (OPC) have been performed for the last several decades (Allen, 2005; Allen and Livingston, 1998; Allen et al., 1987; Allen et al., 2007; Allen et al., 1982). In the last decade, neutron facilities have been able to

provide more intense and brighter sources of neutrons that allow measurements of greater sensitivity, higher speed, and better resolution, which enable examination of the hydration dynamics and kinetics at various time-scales, simultaneously revealing the resulting microstructure of soft and hard matter (Lindroos et al., 2011; Mason et al., 2006). These beamline techniques are more popular and widely used by the biological and materials community, whereas, only limited exposure to these methods is occurring among the cement and concrete research community.

1.1. Importance of next generation instrumental techniques

The multifarious and disordered nature of cement paste spans orders of magnitude from nanometers to millimeters (Biernacki et al., 2017; Provis et al., 2013). The dynamic evolution of hydration products ranges from seconds to years. For example, dissolution reaction occurs in tri-calcium silicate paste in seconds, while the alkali silica reaction(ASR) can take up to several years. Thus, the need for advanced instrumentation is required to accommodate the heterogeneous nature of the complex hydration process. Furthermore, these techniques provide the necessary multi-scale insight and support the initiatives for developing realistic computational models involving crystalline and amorphous hydration products. Recently, these techniques including Quasielastic Neutron Scattering (QENS), Ultra-small X-ray Scattering (USAXS) and Wide Angle X-ray Scattering have been used to investigate the effectiveness of natural pozzolanic additives such as volcanic ash when used as a partial substitute for Portland cement (Kupwade-Patil et al., 2018; Kupwade-Patil et al., 2016b).

1.2. Local additives for cement-based industry

Nowadays, the additives for the cement industry are selected on their availability and demographic regions. For example, fly ash and ground granulated blast furnace slag (GGBFS) are common supplementary cementitious materials used in China, India, USA and Australia; whereas, volcanic ashes are being used in the Middle East region and some parts of Europe. Although, use of local materials as additives is beneficial for the cement industry, associated complexities developed during hydration can result in unreacted products along with a decrease in strength and durability of the resulting cementitious binder.

1.3. Research significance

The current work uses a combination of Small Angle Neutron Scattering (SANS) and Inelastic Neutron Scattering (INS) as a basis for examining resulting microstructure and dynamics when Portland cement is partially replaced by natural pozzolanic volcanic ash. To our knowledge, this is the first time INS has been used in combination with SANS to examine the water dynamics and fractal structure during hydration of Portland cements blended with volcanic ash. Our intention is to provide the information from using these novel techniques to promote discussion and stimulate ideas for further understanding of these complex cementitious material systems.

2. Materials and Methods

2.1. Materials

Type I Ordinary Portland cement (OPC) and volcanic ash from Kingdom of Saudi Arabia were used to prepare combinations of cement paste. The particle size distribution analysis was performed on volcanic ash and OPC by suspending them in isopropyl alcohol using a laser light scattering technique. The particle size analysis of volcanic ash and Portland cement is shown in **Table 1**. Furthermore, the volcanic ash obtained from the manufacturer was ground to a finer size using a high-speed ball mill. The regular volcanic ash that was obtained from the manufacturer was designated as VA1, while the fine ground ash was named as VA2. Throughout the text, the amount (10, 30 or 50 wt%) of OPC replacement by VA1 or VA2 is indicated in the sample terminology. For example, VA1-10 indicates 10 % replacement of OPC by VA1.

Table 1. Particle size analysis for the volcanic ash and ordinary Portland cement (OPC)

Nomination	Mean (μm)	Median (μm)	Mode (μm)	Diameter for Selected percentiles by volume		
				D 90 (μm)	D 50 (μm)	D10 (μm)
VA1	17.14	10.00	13.27	42.46	10.00	1.50
VA2	6.40	3.25	2.97	15.79	3.25	0.97
OPC	12.73	7.94	6.65	30.10	7.94	2.12

2.2. Small Angle Neutron Scattering (SANS)

Small angle neutron scattering (SANS) sample holders consisted of quartz optical cells with an internal spacing of 1 mm and a radius of 12.7 mm. The cement paste was poured into the cells and immediately mounted on the SANS instrument where the sample temperature was maintained at 25^{o}C. SANS data reported in this study was collected at the GP SANS beamline at the High Flux Isotope Reactor (HIFR), Oak Ridge National Laboratory (ORNL) located in Oak Ridge, TN. The timespan between the start of mixing in the chemical laboratory and the start of data collection at the beamline was within two minutes of mixing. The incident neutron wavelength was 6 Å. Data were collected at three sample-to-detector distances (SDD) of 1 m, 4 m and 13 m, together yielding a medium Q-range of 0.0003 Å^{-1} to 0.028 Å^{-1} and high Q-range of 0.004 Å^{-1} to 0.107 Å^{-1}.

The data at each SDD were recorded on a 2D detector, which was later corrected for detector sensitivity, background effects and sample absorption. The scattered intensity was corrected for background detector efficiency and parasitic scattering. The incoherent scattering from the specimens was estimated from the flat background in the high-Q range. The scattered data were calibrated with respect to the incoming beam flux and averaged (circularly) about the incident beam path. The data at each SDD were normalized with respect to each other and merged to get one dataset over the entire Q range. The scattering data were modelled using Porod theory to evaluate the volume and surface fractals. A Q range in the region of 0.06 Å^{-1} < Q <

0.11 $Å^{-1}$ was used for measuring the SANS power law slopes. Data reduction was performed using the SANS macros incorporated in Igor software (Kline, 2006).

The absolute calibrated small-angle scattered intensity, I(Q) was measured over several decades of the scattering vector magnitude, Q (Porod, 1982).

$$Q = \frac{4\pi}{\lambda}\sin\left(\frac{\theta}{2}\right) \quad [1]$$

where λ is the incident wavelength, and θ is the scattering angle

The scattering invariant was calculated by (Allen and Thomas, 2007),

$$Q_{INV} = 2\pi^2\varphi(1-\varphi) * |\Delta\rho|^2 = \int_0^\infty Q^2 \frac{d\Sigma}{d\Omega}(Q)dQ \quad [2]$$

where φ is the solid volume fraction, $\Delta\rho^2$ is the scattering contrast between pores and the solid that can be used for USAXS data. The solid volume fraction is the volume of the solid penetrated by the neutron beam (Trapote-Barreira et al., 2015). It is essentially a measure of the amount of cementitious matrix without considering the gel pores. The standard Irena program package (Ilavsky and Jemian, 2009) along with the model by Allen and Thomas, 2007 (Allen and Thomas, 2007) and Bumrongjaroen *et al*. 2009 (Bumrongjaroen et al., 2009) were used to analyse the SANS scattering data and to obtain the ratio of volume and surface fractals.

The surface fractal surface area, S_{sf}, was extracted by extrapolation of the surface fractal scaling to the minimum applicable length-scale, R_c.

$$S_{SF} = S_0\left(\frac{\xi_s}{R_c}\right)(D_{SF}-2) \quad [3]$$

where R_c is the minimum center-to-center distance between the globules, S_0 refers to the smooth surface area of the surface fractal microstructure,D_{SF} is the surface fractal exponent, ξ_s is the upper limit length scales over which the surface fractal scaling applies. The volume fractal morphology (S_{VF}) was calculated using

$$S_{VF} = S_T - S_{SF} \quad [4]$$

where S_T is the total internal surface area per unit sample volume and S_{SF} is the surface fractal surface area

2.3. Inelastic Neutron Scattering (INS)

The INS measurements were performed at room temperature at the NIST Center for Neutron Research (NCNR) using the BT-4 Filter-Analyzer Neutron Spectrometer (FANS) (Udovic et al., 2008). The samples were all annular-shaped with 12.5 mm nominal annulus diameters. A Cu (220) monochromator was used, with pre- and post-collimations of 60' and 40' and an energy range of 35 meV to 250 meV. The energy resolution (as a percentage of the energy transfer) increased monotonically from around 4 % at 35 meV to around 9 % at 250 meV. Fresh cement pastes were prepared and scans were taken at 45 min time intervals for a total of 1000 min each. The data was reduced and analyzed using DAVE software provided by the NCNR (Azuah et al., 2009).

3. RESULTS AND DISCUSSION

In what follows are results from SANS for examining the microstructural evolution during hydration and investigation of water dynamics via INS experiments.

3.1. Small Angle Neutron Scattering (SANS)

The experimental scattering intensity curves for OPC-VA combination of cement pastes for I(Q) vs Q regime are shown in Figure 1A. A plot on a log-log scale of *I*(Q) vs *Q* for VA1-10, VA1-30 and VA1-50 after 30 min of hydration are shown in Figure 1 B, C and D, respectively. The scattering curve shown in Figure 1A exhibits two scales of interest. The high-*Q* extends between 0.03 Å^{-1} and 0.14 Å^{-1}, where no signs of deviation are observed. The curves show scattering in the high-*Q* regime that is common for detecting fractal systems. The medium-*Q* region of interest extends between 0.03 Å^{-1} and 0.004 Å^{-1}, where VA1-50 shows slightly lower scattering intensity compared to VA1-10 and VA1-30. The fractal model parameters and expressions of the model were adapted from (Bumrongjaroen et al., 2009) and (Allen and Livingston, 1998). As shown in Figures 1A, B and C, volume fractal scaling was attributed to $Q^{-D_{VF}}$ dependence between a *Q* range of Q^{-2} and Q^{-3} for 2 <D_{VF} < 3, and surface fractal scaling was assigned to $Q^{-(6-D_{SF})}$ dependence at low *Q* values (Q^{-3} and Q^{-4} for 2 < D_{SF}<3). Here, the medium Q regime is of importance, since the changes that occur in medium Q reveal critical insights into the mechanism of hydration. From Figure 1A, the drop in the intensity at medium Q for the VA1-50 sample reveals that 50% volcanic ash is not reacting with Portland cement and thus the VA is contributing to the coarseness, which is also observed by an increase in D_{VF} values as shown in Figure 1D.

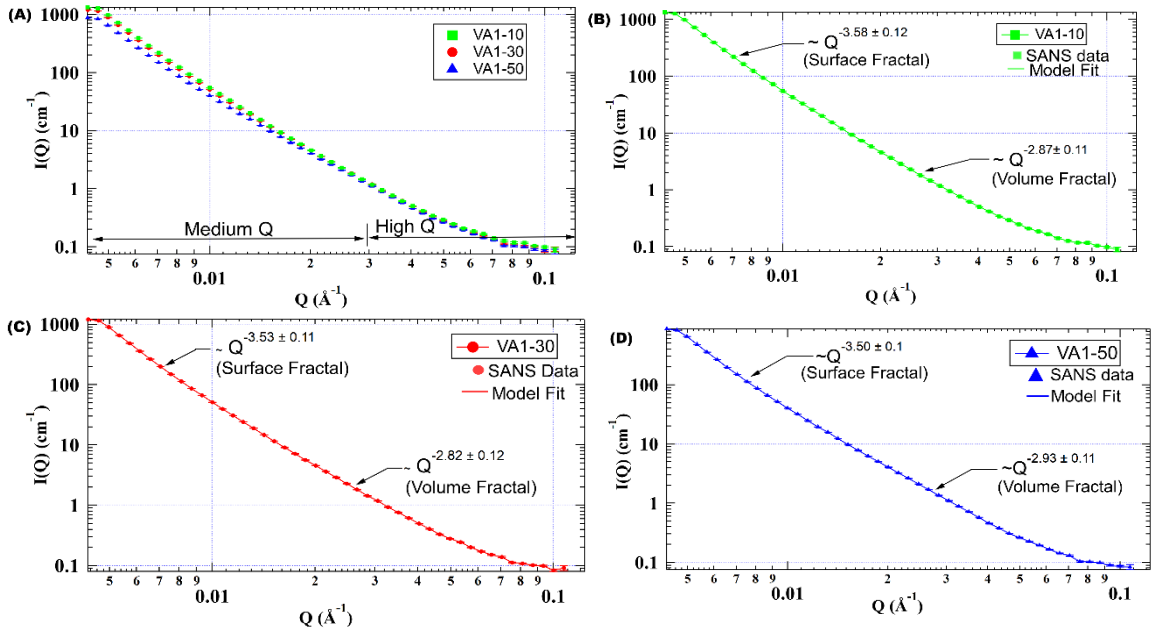

Fig 1. A) SANS plot of scattered neutron scatting intensity *I*(Q) vs neutron wave vector *Q* (Å^{-1}) of three volcanic ash-Portland cement combinations of mixing with 0.55 water to cement ratio after 30 min of hydration. Surface and volume fractal fits for B) VA1-10, C) VA1-30 and D) VA1-50 after 30 min of hydration.

The inverse power-law exponents that vary from 1, 2, or 4 are explained in terms of the concept of fractal (Roe, 2000). A surface with coarseness is known as surface fractal, whereas the blend of mass and surface scale is known as the “mass or volume fractal”(Avnir, 1989). The volume fractal value increases with the addition of volcanic ash, indicating two scenarios after 30 min of hydration: one would be the formation of reaction products due to mixing of volcanic ash with OPC leading to agglomerates of hydration products in free water; the other possibility would be water getting entrapped inside the volcanic ash. This second scenario is more likely to occur when the volcanic ash substitution to OPC is greater than 30 %. In what follows is a detailed Porod plot analysis and fractal study to determine the effect of concentration for optimum replacement of Portland cement with volcanic ash.

Figure 2 illustrates medium-*Q* data for VA1-10 and VA1-50 replotted as IQ^4 vs *Q* (known as a Porod plot), since this helps to enhance the subtle differences during hydration. The data was collected at various times of hydration, with the first data collected after 1 min of mixing. The intensity starts decreasing as the time of hydration increases suggesting a possible surface fractal regime, indicating a $Q^{-3.5}$ as shown in Figure 1B, C and D, **r**espectively. This trend is consistent with the formation of nano-scale C-S-H gel due to hydration and eventually fills the capillary pores, thus minimizing the noticeable surface fractal region in the capillary pores.

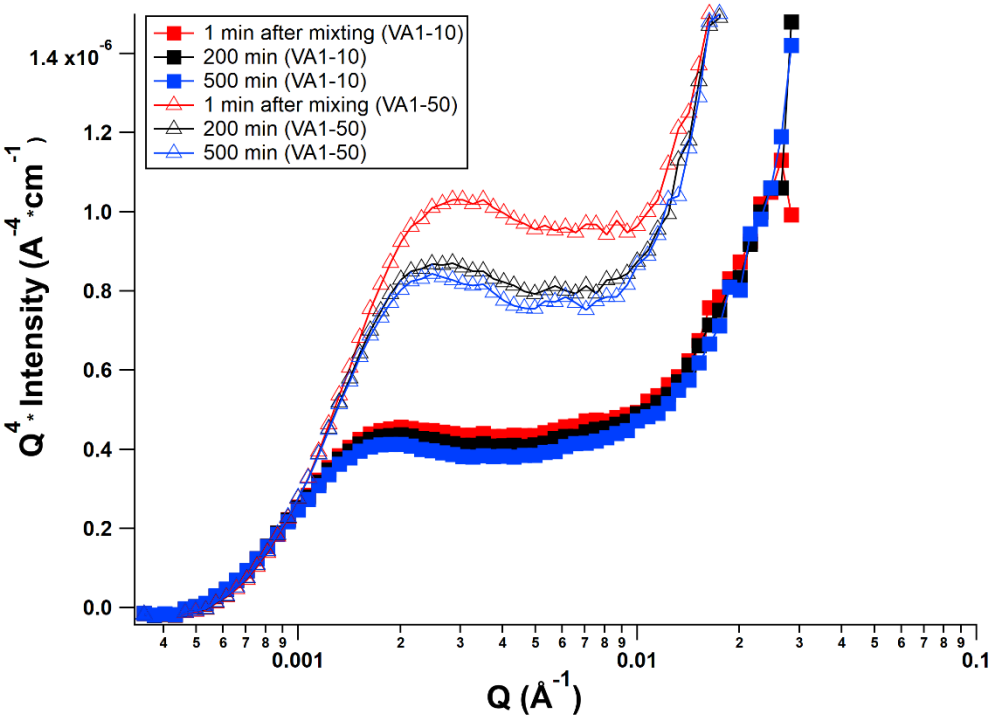

Fig 2. SANS data plotted as I(Q) ×Q^4 versus Q for 10% volcanic ash and 90% Portland cement (VA1-10) after 1 minute of mixing to 560 minutes.

A larger drop in intensity was observed by VA1-50 after 200 min of curing as compared to VA1-10. This suggests that addition of volcanic ash has substantial effect on surface-fractal morphology influencing the formation of C-S-H and other hydration products such as C-A-S-H and M-S-H that were observed in another study (Kupwade-Patil et al., 2016a). Difference in intensities are attributed to different scattering contrast factors that are dependent on scattering length densities of phases initiating

the Porod scattering. The observed much higher drop in intensity after 200 min of hydration for VA1-50 over that for VA1-10 suggests that addition of volcanic ash prevents early-age setting, thus allowing more free water to be available in the system. This was supported by Quasielastic Neutron Scattering (QENS) data for the hydrating cement with volcanic ash (Kupwade-Patil et al., 2016b). Upon 50% substitution the volcanic ash can act as a filler and may not be completely involved in the hydration process. Also, the free water can exist independently inside the unreacted ash and at a later stage may be involved in the formation of nano-crystal zeolites. Additional studies using Ultra-small Angle Neutron Scattering and Neutron Pair Distribution Function (PDF) analysis are required to examine the effect of the base volcanic ash with water. Also, studies using isothermal calorimetry and Nuclear Magnetic Resonance (NMR) relaxometry are required to relate the hydrating rates to the thermodynamic properties of the cement prepared with blends of volcanic ashes.

For the real time early hydration study, Figure 3 presents a plot of volume-fractal (S_{vf}) / surface fractal (S_{sf}) versus hydration time for Portland cement substituted with VA1 (volcanic ash with 17 µm) in 10%, 30% and 50%. Surface fractal deals with the roughness of only surfaces whereas mass fractal deals with mass and surface alike systems (Avnir, 1989; Russ, 2013). At medium *Q* values, the features result from microstructural evolution; in young cement pastes, the original clinker grains are coarsened during the initial hydration process. This suggests that greater than 30% substitution of Portland cement with volcanic ash promotes fractal structure formation along the longer length scales. Furthermore, it also suggests that a smaller quantity of volcanic ash substitution for Portland cement has minimal effect on the region of exponential *Q* dependence.

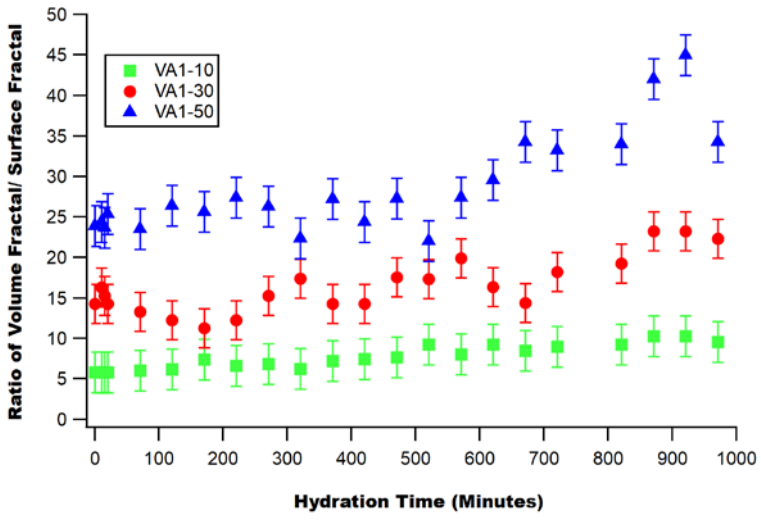

Fig 3. Volume Fractal/Surface Fractal ratio vs hydration time for Portland cement substituted with 10 %, 30% and 50% volcanic ash with 17 µm (VA1)

Additionally, at higher volcanic ash contents, greater contact between OPC and VA occurs, indicating that a higher aluminosilicate source is available to react with water, forming rapid hydration products. These results are similar to the work performed by Allen and Livingston, 1998 (Allen and Livingston, 1998), which shows that addition of silica fume increased the surface area by forming a finer morphology, indicating C-S-H formation. VA has high alumina and magnesium content compared

to OPC, leading to formation of heterogeneous phases consisting of C-S-H, C-A-S-H, and M-S-H (Kupwade-Patil et al., 2016a). Nonetheless, addition of volcanic ash can also generate significant C-S-H and other forms of C-S-H with varying Ca to Si ratios (Massazza, 2002). However, the significant increase in surface area due to 50% volcanic ash content may also be influenced by the net surface area of the volcanic ash itself that is not involved in the formation of C-S-H, C-A-S-H or other related hydration gels. Further studies to examine water dynamics were performed using inelastic neutron scattering by reducing the particle size of the volcanic ash and examining the water effect during the early stages of the hydration process.

3.2. Inelastic Neutron Scattering (INS)

Inelastic neutron scattering spectra at room temperature for water, OPC and VA1 mixed with water are shown in Figure 4. This data was collected after 30 min of mixing with VA1 and OPC with water. For comparison, each dataset was fit with a Gaussian. We can observe that VA1 mixed with water had the least intensity between 50 and 200 meV; meanwhile, water had the highest intensity followed by OPC mixed with water. In these materials, the free liquid water shows enhanced vibrational scattering intensity at lower energies (~60-100 meV), whereas the bound water is more associated with scattering intensity above ~100 meV, although in reality there is considerable overlap between the two.

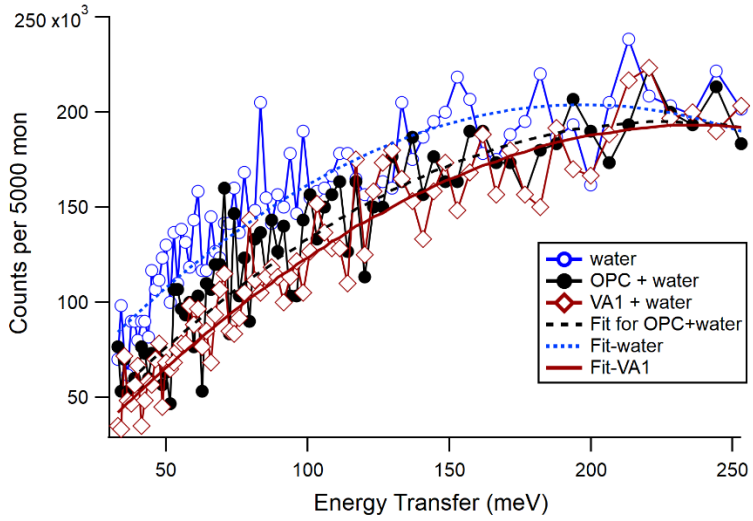

Fig 4. INS spectra of water, Ordinary Portland cement paste and cement paste with volcanic ash

The drop in the intensity at lower energies for OPC and VA indicates that free water is getting utilized to form chemically bound water due to the pozzolanic reaction which occurs due to reaction with water. It is worth noting that VA mixed with water shows slightly reduced intensity compared to OPC due to the rapid dissolution process, since VA is a high source of alumina silicates. The hydration data until 1000 min for OPC, 90% OPC mixed with 10% of VA1 and 90% OPC mixed with 10% of VA2 is shown in Figure 5. Percentage intensity increase with time is shown in Figure 5D.

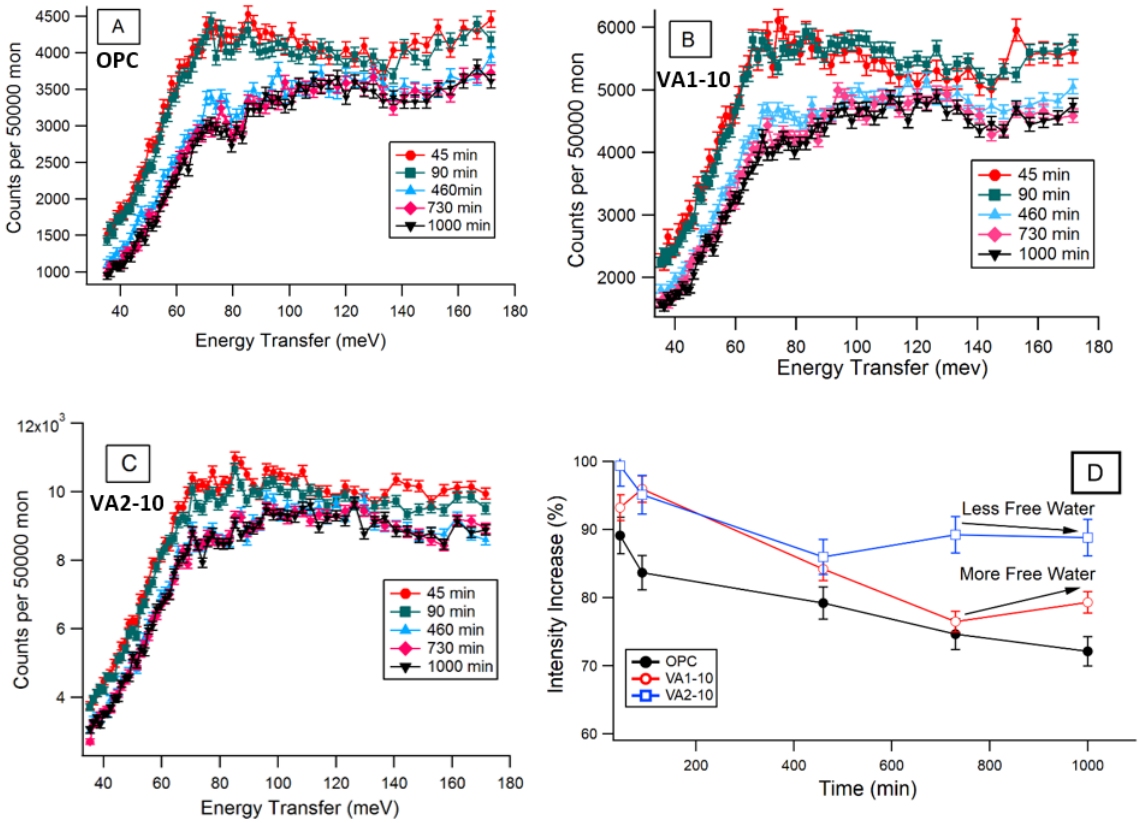

Fig 5. INS spectra with Cu (220) monochromator for hydrating cement paste prepared with (A) OPC, (B) VA1-10 (10% volcanic ash for 17µm and 90% OPC) (C) VA2-10 (10% volcanic ash for 6 µm and 90% OPC). (D) Comparison of intensity analysis for OPC, VA1-10 and VA2-10 at selected times of hydration.

The intensity of OPC sample keeps on decreasing with time, whereas the VA1-10 sample shows an increase in intensity from 45 to 90 min of hydration followed by a decrease in intensity until 730 min followed by a slight increase in intensity at 1000 min. This suggests that the addition of volcanic ash (VA1) promotes active changes during the pre- and post-induction period of hydration. When the volcanic ash was ground from a mean size of 17 µm to 6 µm, the intensity drop was similar to the OPC sample. However, after 460 min, an increase in intensity is observed followed by a decrease. A drop in the intensity of VA1 after 730 min of hydration suggests that free water is still getting utilized to form chemically bound water, forming hydration products. This infers that the volcanic ash being high in alumina, silica and magnesium forms a combination of C-S-H, C-A-S-H and M-S-H gels that influence the setting behaviour of the cement paste. This INS data clearly shows the effect of particle size of volcanic ash and its dominant effect during the course of hydration. Hence, caution has to be exercised when dealing with natural supplementary cementitious materials, as they can be reactive during the course of hydration producing non-uniform and multifarious hydration products.

4. CONCLUSIONS

The paste of highly used materials (Ordinary Portland Cement) in the presence of different percentages (10, 30 and 50%) of high-abundance additives (volcanic ash) was explored, in situ, using powerful and non-invasive techniques (SANS and INS) to better understand the nano- and microstructures arising at early stages of hydration. The microstructure details in terms of fractal morphology were examined via SANS, while the water dynamics was investigated via INS. The data obtained from ratio of Volume Fractal to Surface Fractal clearly shows that greater than 30 % substitution of volcanic ash leads to unreacted volcanic ash and coarser morphology, which could influence the mechanical properties of the resulting hydration products. INS results showed that the effect of finer-particle-sized volcanic ash contributes to uniform hydration which accommodates higher conversion of free water to bound water. Thus, the uses of neutron-based scattering techniques provide critical insights into the hydration dynamics along with morphological information as a basis for engineering natural supplementary cementitious materials for use in Portland-cement-based systems.

REFERENCES

Allen, A.J., 2005. Characterization of Ceramics by X-Ray and Neutron Small-Angle Scattering. Journal of the American Ceramic Society 88, 1367-1381.

Allen, A.J., Livingston, R.A., 1998. Relationship between differences in silica fume additives and fine-scale microstructural evolution in cement based materials. Advanced Cement Based Materials 8, 118-131.

Allen, A.J., Oberthur, R.C., Pearson, D., Schofield, P., Wilding, C.R., 1987. Development of the fine porosity and gel structure of hydrating cement systems. Philosophical Magazine Part B 56, 263-288.

Allen, A.J., Thomas, J.J., 2007. Analysis of C–S–H gel and cement paste by small-angle neutron scattering. Cement and Concrete Research 37, 319-324.

Allen, A.J., Thomas, J.J., Jennings, H.M., 2007. Composition and density of nanoscale calcium-silicate-hydrate in cement. Nat Mater 6, 311-316.

Allen, A.J., Windsor, C.G., Rainey, V., Pearson, D., Double, D.D., Alford, N.M., 1982. A small-angle neutron scattering study of cement porosities. Journal of Physics D: Applied Physics 15, 1817-1834.

Avnir, D., 1989. The Fractal Approach to Heterogeneous Chemistry: Surfaces, Colloids, Polymers. Wiley.

Azuah, R.T., Kneller, L.R., Qiu, Y., Tregenna-Piggott, P.L.W., Brown, C.M., Copley, J.R.D., Dimeo, R.M., 2009. DAVE: A comprehensive software suite for the reduction, visualization, and analysis of low energy neutron spectroscopic data. Journal of Research of the National Institute of Standards and Technology 114, 341-358.

Biernacki, J.J., Bullard, J.W., Sant, G., Brown, K., Glasser, Fredrik P., Jones, S., Ley, T., Livingston, R., Nicoleau, L., Olek, J., Sanchez, F., Shahsavari, R., Stutzman, P.E., Sobolev, K., Prater, T., 2017. Cements in the 21st century: Challenges, perspectives, and opportunities. Journal of the American Ceramic Society 100, 2746-2773.

Bumrongjaroen, W., Livingston, R.A., Neumann, D.A., Allen, A.J., 2009. Characterization of fly ash reactivity in hydrating cement by neutron scattering. Journal of Materials Research 24, 2435-2448.

Ilavsky, J., Jemian, P.R., 2009. Irena: tool suite for modeling and analysis of small-angle scattering. Journal of Applied Crystallography 42, 347-353.

Kline, S., 2006. Reduction and analysis of SANS and USANS data using IGOR Pro. Journal of Applied Crystallography 39, 895-900.
Kupwade-Patil, K., Al-Aibani, A.F., Abdulsalam, M.F., Mao, C., Bumajdad, A., Palkovic, S.D., Büyüköztürk, O., 2016a. Microstructure of cement paste with natural pozzolanic volcanic ash and Portland cement at different stages of curing. Construction and Building Materials 113, 423-441.
Kupwade-Patil, K., Chin, S., Ilavsky, J., Andrews, R.N., Bumajdad, A., Büyüköztürk, O., 2018. Hydration kinetics and morphology of cement pastes with pozzolanic volcanic ash studied via synchrotron-based techniques. J Mater Sci 53, 1743-1757.
Kupwade-Patil, K., Tyagi, M., Brown, C.M., Büyüköztürk, O., 2016b. Water dynamics in cement paste at early age prepared with pozzolanic volcanic ash and Ordinary Portland Cement using quasielastic neutron scattering. Cement and Concrete Research 86, 55-62.
Lindroos, M., Bousson, S., Calaga, R., Danared, H., Devanz, G., Duperrier, R., Eguia, J., Eshraqi, M., Gammino, S., Hahn, H., Jansson, A., Oyon, C., Pape-Møller, S., Peggs, S., Ponton, A., Rathsman, K., Ruber, R., Satogata, T., Trahern, G., 2011. The European Spallation Source. Nuclear Instruments and Methods in Physics Research Section B: Beam Interactions with Materials and Atoms 269, 3258-3260.
Mason, T.E., Abernathy, D., Anderson, I., Ankner, J., Egami, T., Ehlers, G., Ekkebus, A., Granroth, G., Hagen, M., Herwig, K., Hodges, J., Hoffmann, C., Horak, C., Horton, L., Klose, F., Larese, J., Mesecar, A., Myles, D., Neuefeind, J., Ohl, M., Tulk, C., Wang, X.L., Zhao, J., 2006. The Spallation Neutron Source in Oak Ridge: A powerful tool for materials research. Physica B: Condensed Matter 385-386, 955-960.
Massazza, F., 2002. Properties and applications of natural pozzolanas, Structure and Performance of Cements, pp. 326-352.
Porod, G., 1982. General theory, Small angle X-ray scattering.
Provis, J.L., Hajimohammadi, A., White, C.E., Bernal, S.A., Myers, R.J., Winarski, R.P., Rose, V., Proffen, T.E., Llobet, A., van Deventer, J.S.J., 2013. Nanostructural characterization of geopolymers by advanced beamline techniques. Cement and Concrete Composites 36, 56-64.
Roe, R.J., 2000. Methods of X-ray and Neutron Scattering in Polymer Science. Oxford University Press.
Russ, J.C., 2013. Fractal Surfaces. Springer US.
Trapote-Barreira, A., Porcar, L., Cama, J., Soler, J.M., Allen, A.J., 2015. Structural changes in C–S–H gel during dissolution: Small-angle neutron scattering and Si-NMR characterization. Cement and Concrete Research 72, 76-89.
Udovic, T.J., Brown, C.M., Leão, J.B., Brand, P.C., Jiggetts, R.D., Zeitoun, R., Pierce, T.A., Peral, I., Copley, J.R.D., Huang, Q., Neumann, D.A., Fields, R.J., 2008. The design of a bismuth-based auxiliary filter for the removal of spurious background scattering associated with filter-analyzer neutron spectrometers. Nuclear Instruments and Methods in Physics Research Section A: Accelerators, Spectrometers, Detectors and Associated Equipment 588, 406-413.

ACKNOWLEDGEMENT

We acknowledge the support of the National Institute of Standards and Technology, U.S. Department of Commerce, in providing neutron research facilities used in this work. This research also used resources at the High Flux Isotope Reactor (HFIR), a Department of Energy (DOE) Office of Science User Facility operated by the Oak Ridge National Laboratory. We thank the “Kuwait Foundation for the Advancement of Sciences (KFAS)” for their support during this work.